A R C H I V E S O F M E T A L L U R G Y A N D M A T E R I A L S
Volume 54 2009 Issue 1

H. PAUL[*,**], J. DRIVER[***], C. MAURICE[***], M. MISZCZYK [**], D. PIOT[***]

DEFORMATION MICROSTRUCTURE AND TEXTURE EVOLUTION OF {110}<112> Al-0.3wt.%Mn SINGLE CRYSTALS COMPRESSED IN A CHANNEL-DIE

EWOLUCJA TEKSTURY I MIKROSTRUKTURY NIESWOBODNIE ŚCISKANYCH MONOKRYSZTAŁÓW STOPU {110}<112> Al-03wag.%Mn

Crystal subdivision patterns of microbands have been extensively reported but mostly by studies on only one section, using either TEM or SEM-EBSD. To better correlate substructure with slip patterns a systematic study of the 3D deformation microstructure in a deformed single crystal (i.e. over the 3 perpendicular surfaces) has been carried out. The microstructure and microtexture evolutions during plane strain deformation of high purity single crystals of Al-0.3%wt.Mn alloy with initial ideal and near-brass{110}<112> orientations were characterised by TEM and high resolution FEG-SEM/EBSD after strains of 0.15 and 0.56. These two different techniques enable one to examine the crystal subdivision deformation pattern at different microscopic scales, on the 3 orthogonal sections, i.e. perpendicular to the nominal <110>, <112> and <111> crystallographic directions. Particular attention is paid to a comparison of the microband orientations with the expected slip traces of the 2 active slip systems on all 3 surfaces. It is concluded that the microband boundary alignment corresponds very well to the traces of the crystallographic {111} planes, on which most of the slip occurs.

Keywords: Texture, microstructure, Al-Mn alloy, orientation mapping, microbands

W pracy przedstawiono wyniki badań eksperymentalnych rozwoju tekstury i struktury dyslokacyjnej w nieswobodnie ściskanych monokryształach stopu Al-0.3wag. % Mn o orientacji {110}<112> (idealnej oraz 'odchylonej' ~ 3° od położenia idealnego, drogą obrotu dookoła kierunku wypływania), na trzech wzajemnie prostopadłych przekrojach. Badania zmian struktury dyslokacyjnej prowadzono z wykorzystaniem elektronowej mikroskopii transmisyjnej (TEM) i skaningowej (SEM) a zmian teksturowych z wykorzystaniem technik pomiaru orientacji lokalnych w TEM i SEM wyposażonego w działo o emisji polowej, dla dwu stopni odkształcenia, tj. 0.15 i 0.56 (odkształcenie logarytmiczne). Obydwie zastosowane techniki umożliwiają analizę formowania się struktury dyslokacyjnej i procesu jej fragmentacji wraz z odkształceniem na trzech ortogonalnych przekrojach, prostopadłych do kierunków krystalograficznych <110>, <112> oraz <111>. Szczególną uwagę zwrócono na porównanie usytuowania przestrzennego struktury mikropasm z usytuowaniem aktywnych śladów poślizgów na trzech wzajemnie prostopadłych przekrojach. Stwierdzono, że dyslokacyjne granice mikropasm bardzo dobrze korespondują z usytuowaniem śladów dwu płaszczyzn {111} na których działają dwa najbardziej uprzywilejowane systemy poślizgu.

1. Introduction

Microstructure and texture development during deformation of face centered cubic (fcc) metals and alloys has been extensively analyzed over the last years. In metals with medium-high stacking fault energy two main types of planar microstructures are observed and can have a strong influence on materials properties, e.g. strength and texture control in metal forming. They are microbands, dominating microstructure development at low deformations and micro/macro shear bands, most frequently observed after high strain at low temperatures. The purpose of this study is to characterize the development of microbands during deformation in relation to the active slip systems.

For the particular case of plane strain compression the slip pattern distribution and local lattice reorientations as measured by either transmission electron microscopy (TEM) and scanning electron microscopy equipped with electron backscatteved diffraction facilities (SEM-EBSD) on the ND-ED plane (where: ND and ED – normal and extension directions, respectively)

[*] INSTYTUTE OF METALLURGY AND MATERIALS SCIENCE, POLISH ACADEMY OF SCIENCES, 30-059 KRAKÓW, 25 REYMONTA STR., POLAND
[**] OPOLE UNIVERSITY OF TECHNOLOGY, MECHANICAL DEPARTMENT, POLAND
[***] ECOLE DES MINES DE SAINT ETIENNE, CENTRE SMS, FRANCE

can only give an unequivocal description of the active slip systems when their slip planes contain the transverse direction (TD). In any other case, it is difficult to define precisely the spatial distribution of the active slip systems using only one section, e.g. the longitudinal section. This is particularly important in the debate over the boundary alignment and whether the slip patterns are oriented along crystallographic planes or are primarily a function of the deformation mode.

Evidence for crystallographic alignment of microband boundaries with the slip planes has been presented many times in the past, and is supported by the RISØ group, e.g. [1-6]. They stated that the preference for boundary orientations to develop close to the highly stressed planes (i.e. inclined at 45°) is weaker than the crystallographic preference. However, perfect parallelism is often not observed for these boundaries, and the observed spread in the alignment is very often larger than the orientation changes within the same area. Additionally, even in the cases where close alignment of boundaries with {111} planes may exist in one plane section, the same boundaries may be wavy and irregular in another section. This directly leads to another idea, advocated by the Manchester group, e.g. [7-10], according to which the alignment of low angle boundaries is primarily a function of the deformation mode, rather than crystallography; microbands should align on the planes of maximum shear stress. This leads to the conclusion that only an analysis on three orthogonal planes can fully characterize the spatial dislocation arrangements.

In the past crystal subdivision patterns of microbands have been extensively reported but mostly by studies on only one section, using either TEM or SEM-EBSD. In this work in order to better correlate the substructure with slip patterns, initial and final crystal orientation, and the macroscopic coordinate system, a systematic study of the 3D deformation microstructure (i.e. over the 3 perpendicular surfaces) in a plane strain compressed Al-0.3wt.%Mn single crystal with brass$\{110\}<112>$ orientation, was carried out. It has been pointed out [4] that the brass orientation should be a critical test of whether or not the microband boundary alignment is related to crystallography or to the deformation mode (in opposition to Goss$\{110\}<001>$ orientation, where highly privileged slip systems are operating on {111} planes situated parallel to TD [11]). The ideal brass orientation, stable in channel-die compression up to very high deformations, possesses two major slip systems with planes inclined at ±30° to ED and intersecting the compression plane at 55° to ED.

In fact, one of the initial crystal orientation used here was 'non-ideal' and shifted (+)3° from the ideal position by rotation around ED. Crystal plasticity calculations, e.g. [1] for orientations rotated a few degrees about ED‖<112> axis indicate that some further rotation away from ideal brass should occur during channel-die compression. The present study therefore examines this case in detail.

2. Materials and methods

A single phase Al-0.3%wt.Mn alloy single crystal with near-brass $(\bar{1}01)[1\ \bar{2}\ 1]$ orientation was prepared as follows. A high purity bar with controlled orientation was grown by a modified Bridgman technique (horizontal solidification), using a split graphite mould. Samples with dimensions of 7mm × 7mm × 15mm were carefully machined by spark erosion from the as-grown ingots and compressed in channel-die in a Schenk servo-hydraulic machine at a strain rate of $\sim 10^{-2}s^{-1}$ using Teflon lubrication. The orientations of the crystals before compression were checked by back reflexion Laue X-ray. They were found to be ideal (within 1° of ideal brass) and shifted (+)3° from the ideal position by rotation around ED.

The microstructure and the microtexture evolutions during plane strain deformation were characterized by TEM and high resolution FEG-SEM/EBSD after strains of 0.15 and 0.56. These two different techniques enable one to examine the crystal subdivision deformation pattern at different microscopic scales, on the 3 orthogonal sections, perpendicular to the $[\bar{1}\ 0\ 1]$, $[1\ \bar{2}\ 1]$ and $[\bar{1}\bar{1}\bar{1}]$ crystallographic directions from areas close to the centre of the sample. Particular attention is paid to a comparison of the microband orientations with the expected traces of the active slip systems on all 3 surfaces. The deformed specimens were mostly examined by SEM in a JEOL JSM 6500F equipped with a field emission gun (FEG) and electron backscattered diffraction (EBSD) facilities, where microscope control, pattern acquisition and solution were performed with the HKL Channel 5 system (step size of 100nm). The samples were also examined by TEM using a 200kV Philips TEM CM200 and convergent beam electron diffraction (CBED) with semi-automatic Kikuchi pattern analysis. The thin foils were prepared by twin-jet technique, using TenuPol-5, in a standard solution composed of 20% nitric acid, 75% methanol and 5% of glycol, at -35°C and a voltage of 20-21V. Local orientation data, obtained by TEM and SEM/EBSD techniques are presented in the form of {111} pole figures.

3. Results and discussion

3.1. Slip systems and macroscopic sample changes

The active slip planes in the ideal Bs{110}<112> (or brass) position shown in Fig. 1, were inclined ±30° to ED and intersected the compression plane at the angle of 54.7° in respect to the ED. The traces of active slip systems operating on these planes in 3 orthogonal sections are presented in Figure 2. Based on the Schmid factor calculations it can be seen that slip should be distributed equally and occur predominately on just two systems operating on $(\bar{1}\bar{1}1)$ and $(\bar{1}\ 1\ 1)$ planes.

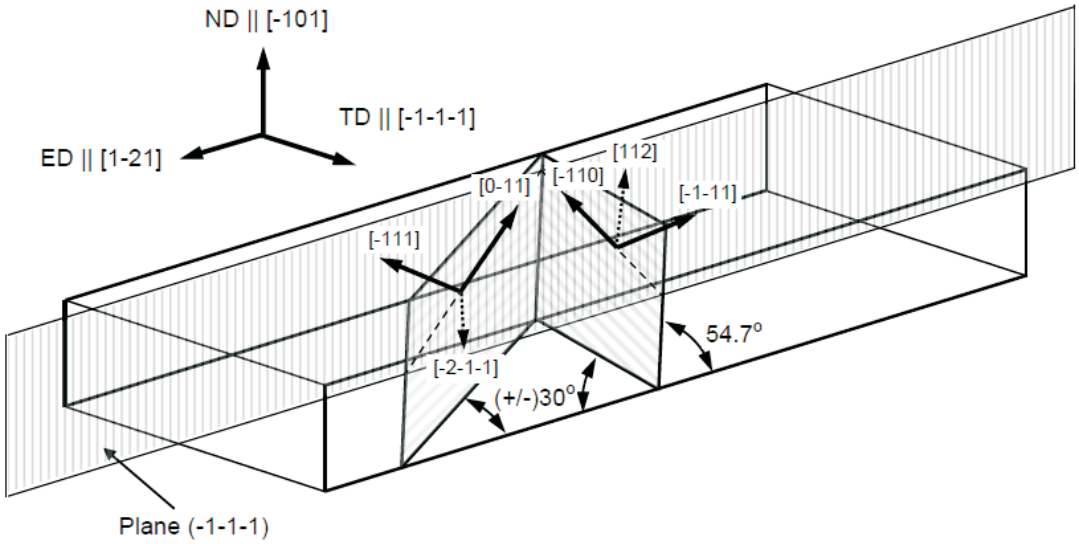

Fig. 1. Schematic presentation of orientations and the active {111} slip planes with respect to the sample axes

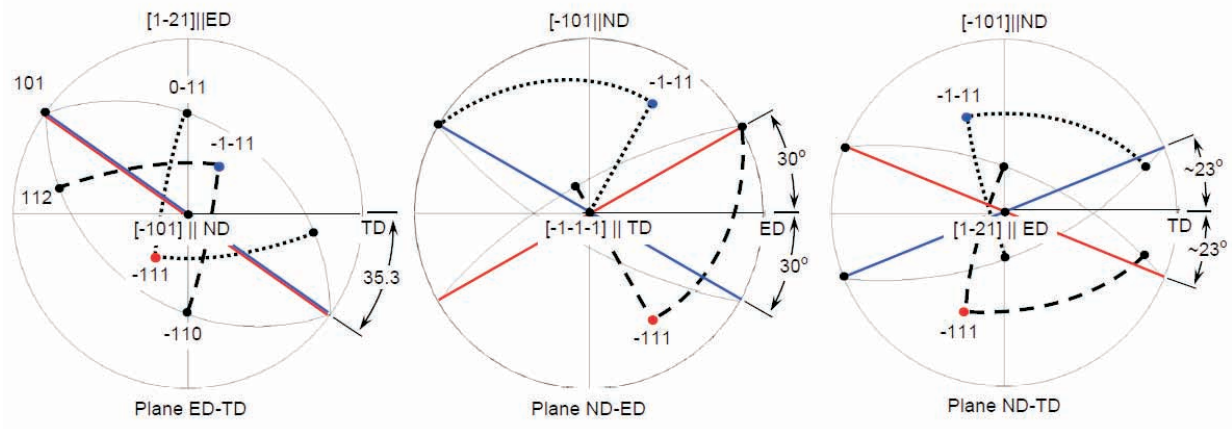

Fig. 2. Stereographic projections on (a) – ($\bar{1}$ 0 1), (b) – $(\bar{1}\bar{1}\bar{1})$ and (c) – (1 $\bar{2}$ 1) planes showing configuration of the most active slip systems in ideal brass($\bar{1}$ 0 1)[1 $\bar{2}$ 1] orientation

Figure 3 shows the macroscopically observed shape changes of the Bs crystals. As expected the crystal undergoes a macroscopic (negative) ε_{xy} shear, typical of plane strain compressed Bs crystals. Standard crystal plasticity predicts this shear as a consequence of slip on the $(\bar{1}\bar{1}$ 1)[$\bar{1}$ 1 0] and ($\bar{1}$ 1 1)[01 $\bar{1}$] (b3 and c1) systems. For the ideal Bs orientation these two systems have equal amplitudes and their lattice rotations balance out to zero rotation up to large strains. For the 3° ED rotated Bs orientation slip occurs on the same systems but the b3 system is favoured compared with c1 (amplitude about twice that of c1) so that non-zero lattice rotation develops about an axis near [212], typically of order 4-5° at a strain of 0.6. Due to the off-ideal orientation a second ε_{xz} shear should also occur. Note that experimentally a "neutral zone" is observed on the top surface (Fig.3b) with traces of intense slip inclined at 25° to TD. Additionally, at deformations of 0.56, the longitudinal section shows signs of weak deformation bands.

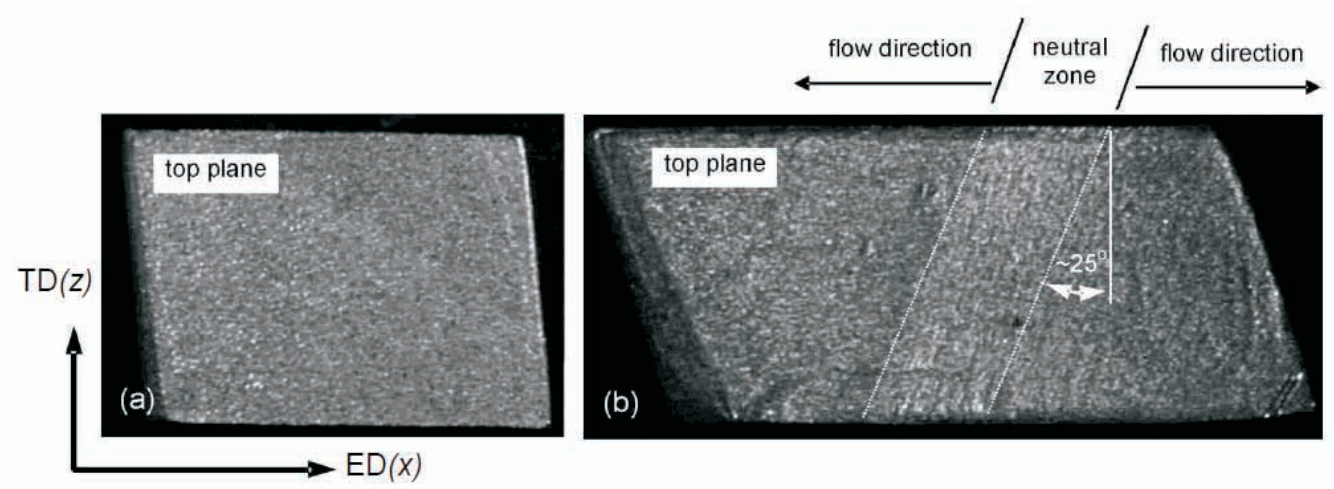

Fig. 3. The shape changes of brass{110}<112> oriented single crystal after deformations of 0.15 (a) and 0.56 (b). Optical micrographs on non-etched sample

The experimentally measured true stress-strain curves, such as the one presented in Figure 4 demonstrate a monotonic increase in stress as a function of strain. The two strong stress relaxations are due to unloading of the sample for changing the Teflon film. These events are manifested on the stress-strain curve as evident separate stress drops.

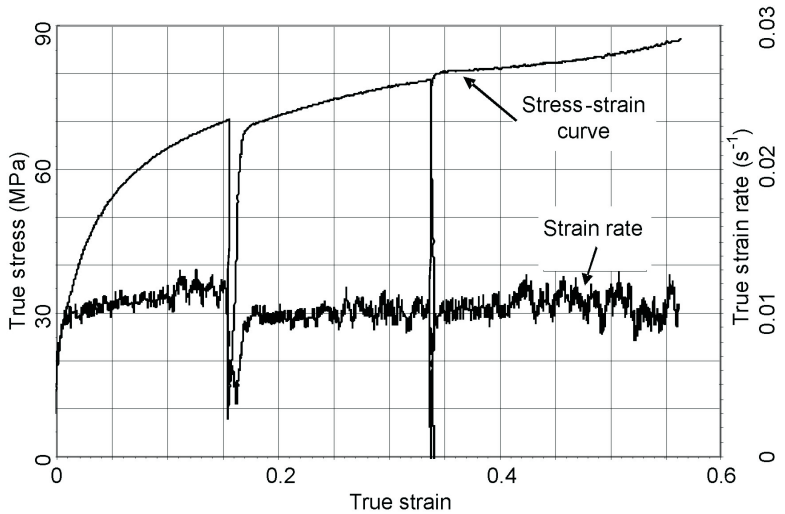

Fig. 4. Stress-strain curve of sample 3° rotated around ED, plane strain compressed 0.56. Stress and strain were calculated as usual by $\sigma = F/A$ and $\varepsilon = ln(ho/h)$, where F, A, h_o, h are the current compression load, sample compression surface area, and initial and current specimen thicknesses, respectively

3.2. SEM-FEG/EBSD microstructure and texture

3.2.1. Low deformation (0.15)

SEM-FEG/EBSD local orientation measurements at a deformation of 0.15 show only slight scattering of the initial orientation and no clearly marked low angle boundaries are observed. This is independent of the analyzed section. The {111} pole figures corresponding to orientation maps made from different areas on the compression plane clearly show little orientation scattering (Fig.5a). Orientations measured on the ND-ED and ND-TD planes also confirm that at low deformations there is little change of the initial orientation (Figs.5b and c).

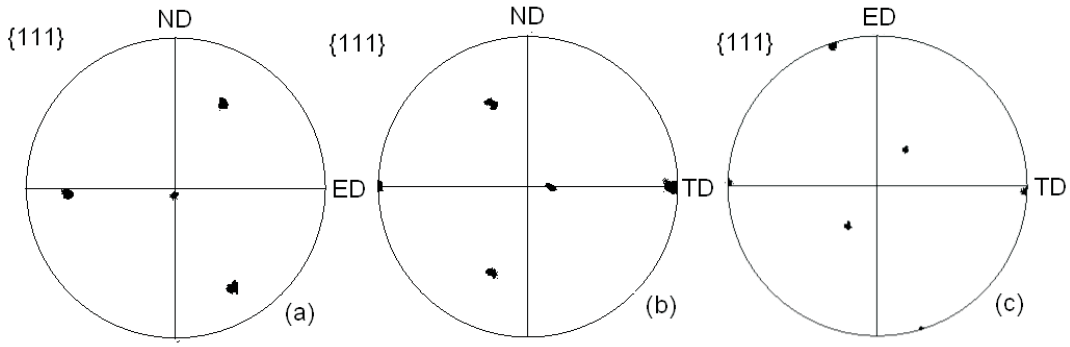

Fig. 5. {111} pole figures showing orientation changes measured in three orthogonal planes at a deformation of 0.15: (a) ND-ED (b) ND-TD, and (c) ED-TD planes. SEM-FEG/EBSD measurements on area of 100μm × 80μm with step size of 100nm

3.2.2. Medium deformation (0.56)

At higher deformations low angle boundaries of one family are clearly visible. The inclination of this characteristic substructure of strongly elongated microbands, with respect to the external directions, depends on the sections. However, strong coincidence with the traces of {111} plane is observed.

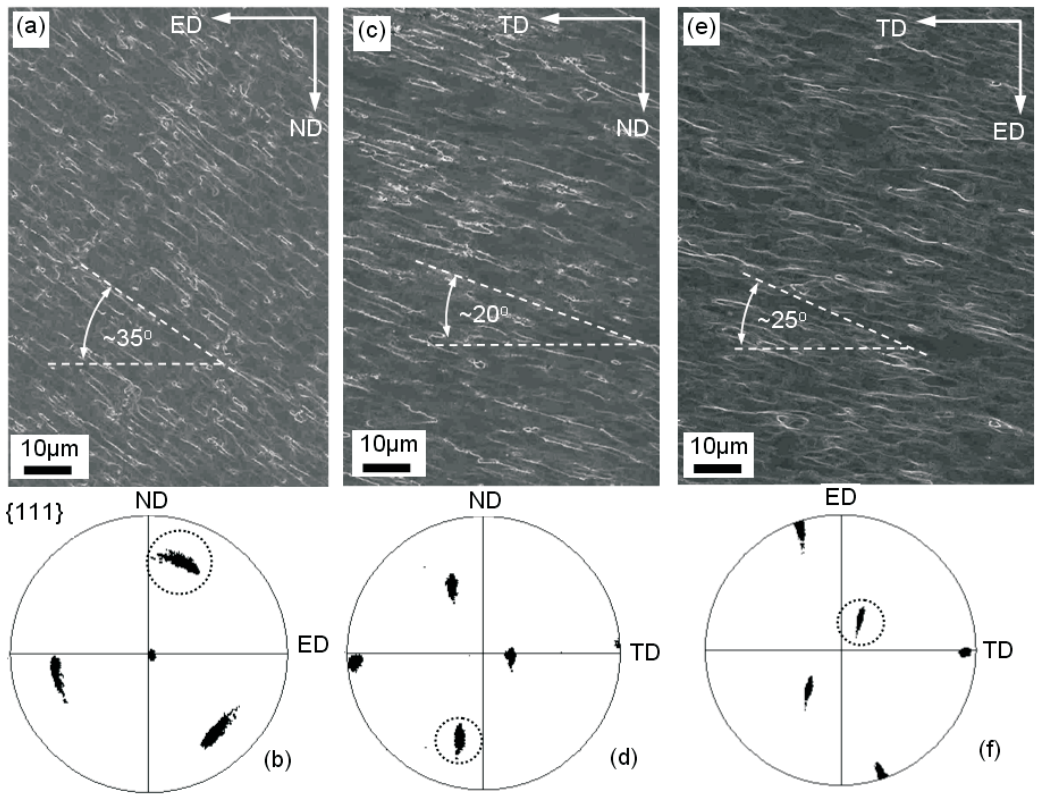

Fig. 6. Maps of adjacent misorientations presented the acquisition planes: (a) ND-ED, (c) ND-TD and (e) ND-TD planes, and (b), (d) and (f) corresponding {111} pole figures, respectively. SEM-FEG/EBSD measurements with step size of 100nm after deformation of 0.56. Gray linear scale is used for presentation of the misorientation between points; regions in white had misorientations above 1.5°. Dotted circle marks poles of the most active $(\bar{1}\bar{1}\ 1)$ slip planes

ND-ED section – longitudinal plane. By optical microscopy this section shows the formation of large blocks divided by broad bands (probably as a result of lubrication). The adjacent misorientation maps made within each area clearly show the domination of one set of microbands, as a result of dislocation activity on the $(\bar{1}\bar{1}1)$ plane in the $[\bar{1}\ 1\ 0]$ direction. High resolution orientation mapping show that the dislocation walls observed in lon-

gitudinal sections are inclined at ~ 35° to ED (Fig.6a). Occasionally some microbands resulting from dislocation motion in the [0 $\bar{1}$ 1] direction along (1$\bar{1}\bar{1}$) planes are observed. The {111} pole figure of Fig.6b shows very strong scattering of the initial orientation. The stability of the [111] pole lying close TD suggests a rotation of the crystal lattice around an axis near to [112] (also lying close to TD) as a result of dislocation slip on the ($\bar{1}\bar{1}$ 1)[$\bar{1}$ 1 0] system.

ND-TD section. In the plane perpendicular to ED also only one set of extended microbands is observed. These bands are inclined at ~20° to TD (Figs.6c). A second set of shorter microbands situated nearly symmetrically to the previous one, is observed occasionally. The corresponding {111} pole figure (Fig.6d) shows orientation scattering essentially about TD, as described above.

ED-TD section (compression plane). In this plane the misorientation maps reveal the formation the elongated boundaries inclined at ~ 20−25° to TD (Fig.6e). A comparison of the orientation changes observed on the {111} pole figures from different areas of the sample shows ~ 10 − 15° difference in the maximum density of <111> poles. An orientation map from the middle layer of the sample shows (Fig.6f) a relatively large orientation scattering (~ 20°), typically observed for unstable orientations. Rotation of the crystal lattice occurs around the axis close to TD, and leads the initial orientation towards {112}<110>.

The crystallite subdivision in the macro scale was analysed in the ED-TD plane. Separate orientation maps were made in different places of the sample, as it is marked in Fig. 7. The comparison of the orientation changes observed in the {111} pole figures from different areas of the sample shows ~ 5° difference in the maximum density of <111> poles.

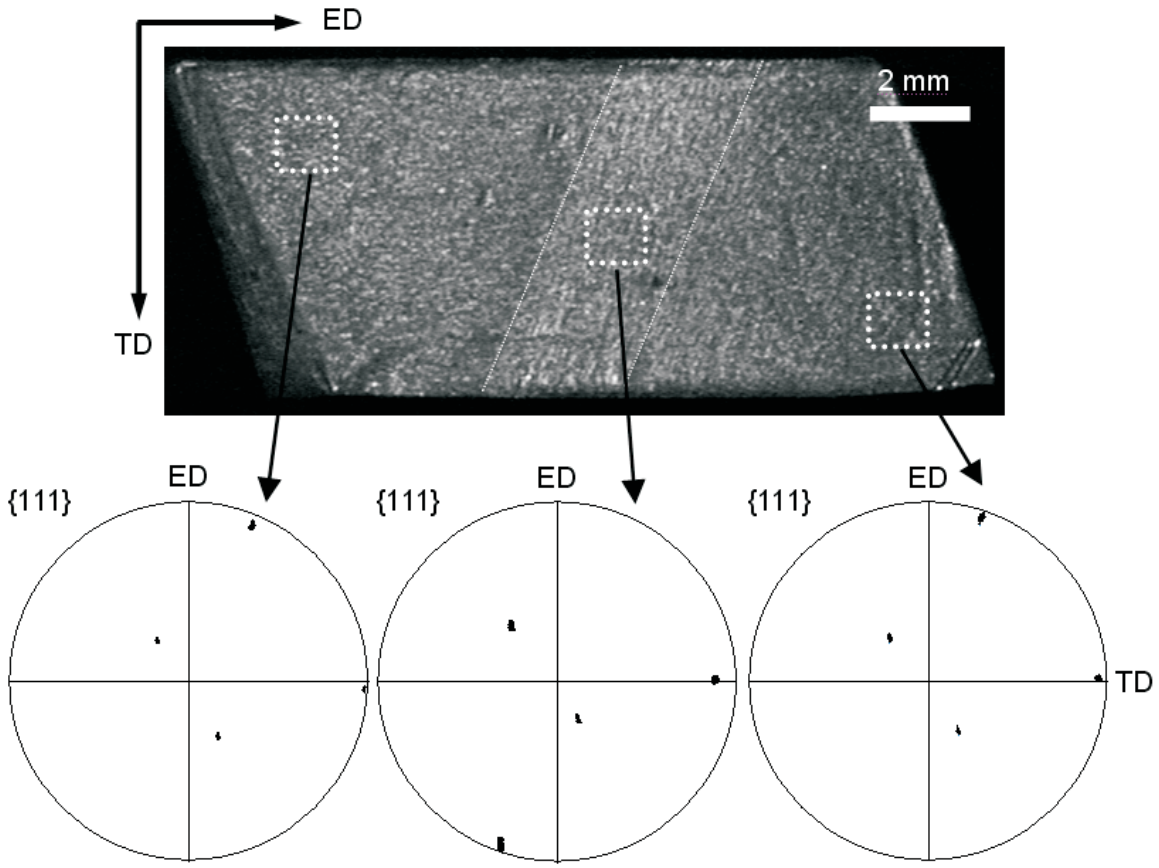

Fig. 7. {111} pole figures showing orientation changes measured in three places of ED-TD plane at a deformation of 0.56. SEM-FEG/EBSD measurements on area of 10μm × 8μm with step size of 100nm

3.3. Misorientation distribution

Misorientation line scans were also performed along particular directions, in all 3 analysed sections, as shown in Fig.8. At the lower deformation all analyzed points had orientations close to the initial one (misorientation angles very rarely exceed a few degrees) and the misorientation profile generally did not show any obvious

tendency. At the higher deformation the scatter of the misorienation line scans increases significantly and a near-cyclic variation of the misorientation angle is clearly observed (Fig.8.). In this case the amplitude attains 10°, and in some cases even 15-20°.

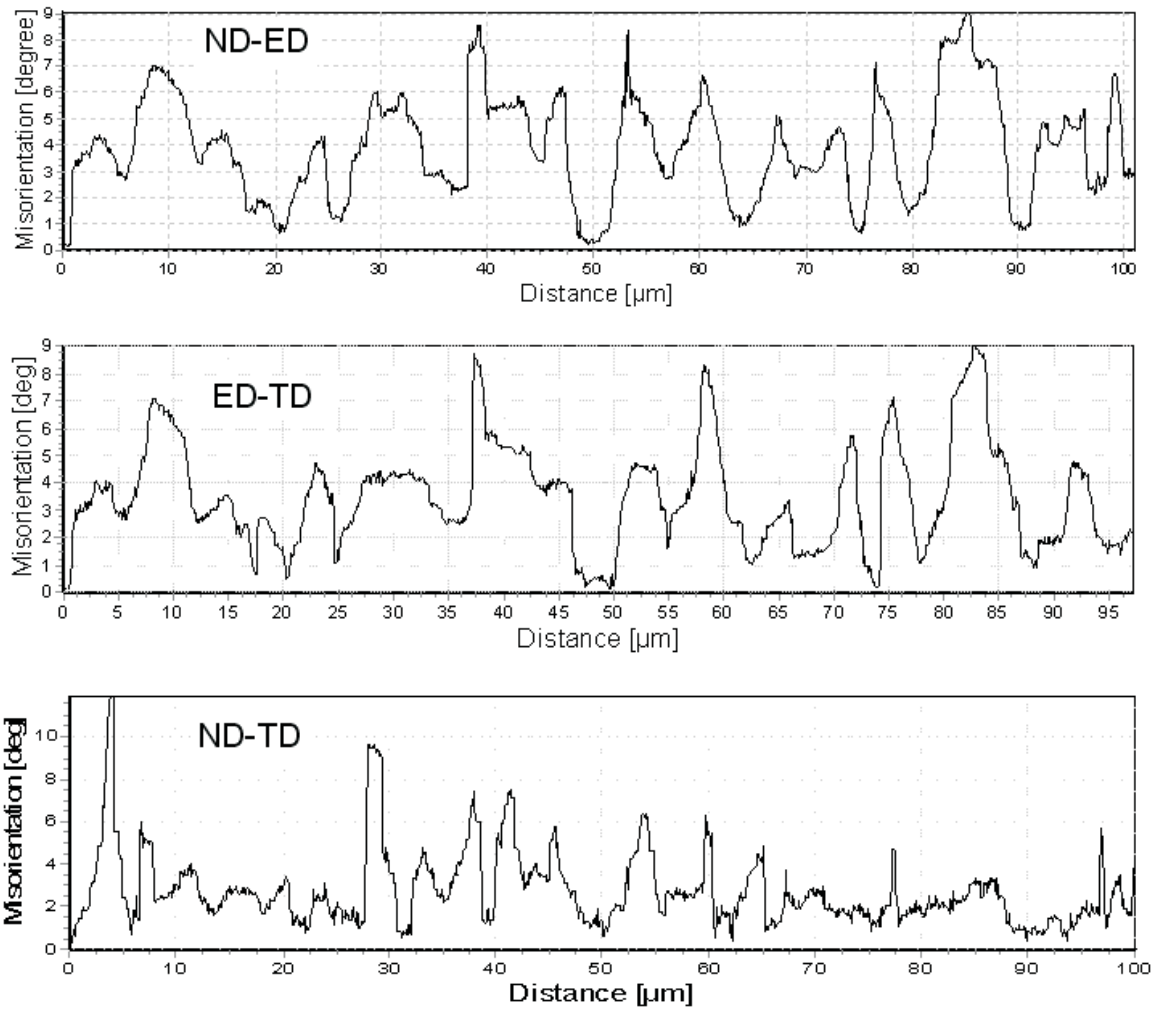

Fig. 8. Local misorientation line scan (point to origin) measured in the ND-ED (||ED), ED-TD (||ED) and ND-TD (||ND) sections of the sample deformed to 0.56. SEM-FEG/EBSD measurements with step size of 100nm

3.4. TEM microstructure and microtexture

All the above tendencies of microband arrangement and crystal lattice rotation are confirmed by TEM observations and local orientation measurements and are described here mainly for the deformation of 0.56.

One set of dislocation walls is the most preferred dislocation substructure observed on the ND-ED plane (longitudinal sections) for both deformations (Figs.9a and b). Two sets of intersecting microbands are only seen occasionally but always one set was dominant. The crystallographic character of these bands is confirmed by selected area diffraction and local (Kikuchi) orientation measurements; they correspond closely to the traces of the b3 and c1 systems. Some of the region show relatively high stability of the crystal lattice orientation where the calculated misorientations with respect to the 1st measured point are very low (< 8°). On the other hand other regions show significantly stronger orientation scattering and the spread of <111> poles could be ~ 20°. However, in all analyzed cases the misorientation axes are close to TD.

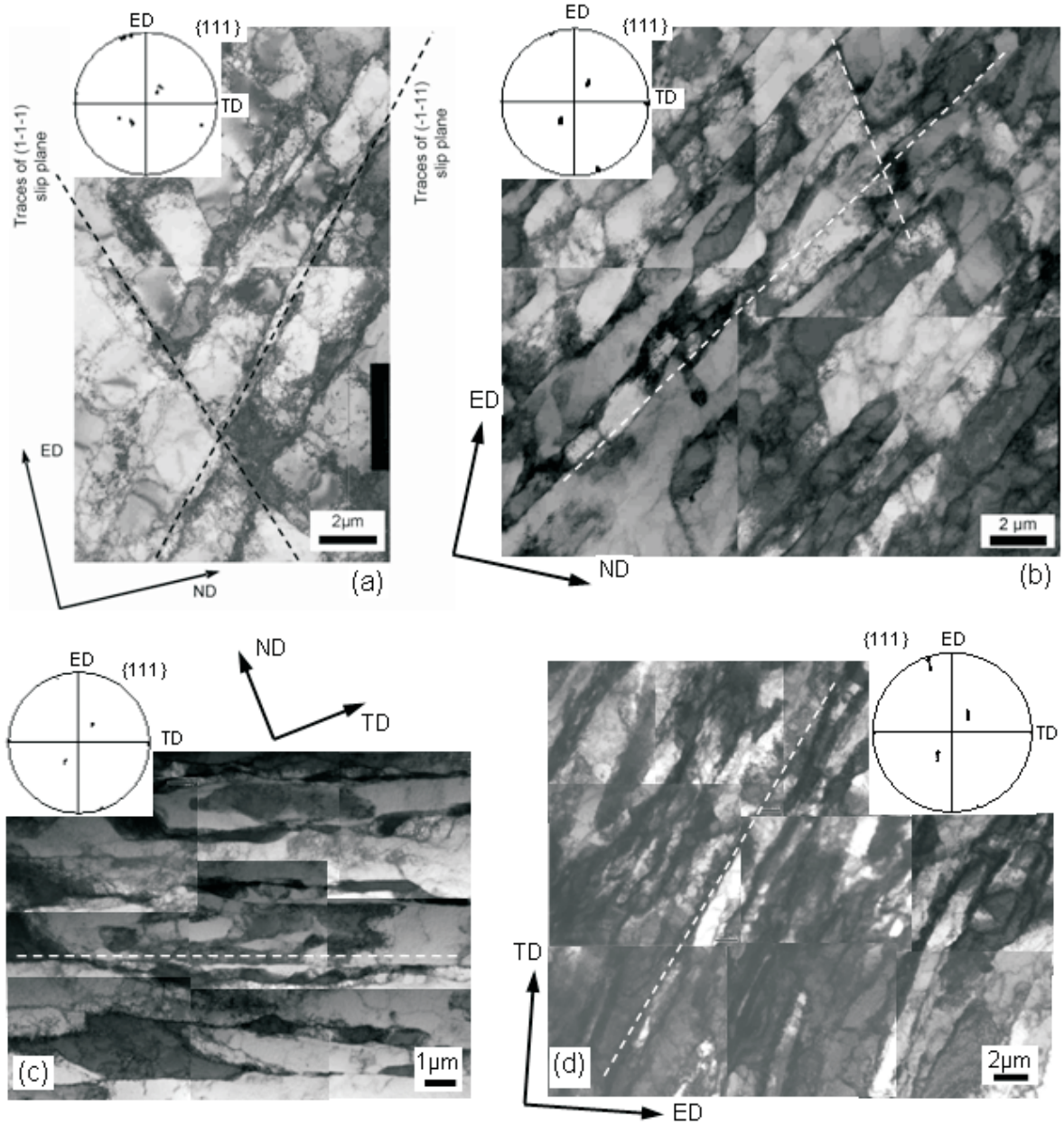

Fig. 9. Typical TEM microstructures and corresponding {111} pole figures showing local orientation changes observed within presented areas: (a) ND-ED section, deformation of 0.15, (b) ND-ED, (c) ED-TD, (d) ND-TD sections, (b)-(d) deformation of 0.56. TEM bright field images and TEM/CBED local orientation measurements

This structural evolution only partly agrees with that seen in TEM foils of rolled Cu single crystals of this orientation as reported by Wróbel et al. [12]. For deformations up to 60% they observed that two sets of dislocation walls existed lying nearly parallel to the traces of the active slip planes, whereas after very high deformations (>95%) only dislocation walls parallel to the rolling direction were observed. The current observations show a structure that may be intermediate between these two cases, as it was previously stated also by Godfrey et al. [1] in their investigations of channel-die compressed pure aluminium.

The second example on the ND-TD plane also shows a tendency, for the dislocation boundaries to lie along directions inclined at ~20-25° to TD (Fig.9c). However, again the local orientation measurements show their crystallographic character, i.e. the boundaries lie close to the predicted traces of {111} planes.

The microstructure observed in the compression plane (plane ED-TD) reveals only a weakly contrasted substructure showing bands inclined at ~25° to TD (Fig.9d). The situation of these bands is approximately parallel to the traces of active $(\bar{1}\bar{1}1)$ slip planes. Local orientation measurements along line scans parallel

to ED shows that some misorientations exceeded 10° with clear non-random misorientation axes distribution. However, higher magnification shows that the walls of the strongly elongated microbands can be very wavy. This is in accordance with results obtained by Godfrey et al [1] which concluded that some of the dislocations within boundaries arise from unpredicted slips.

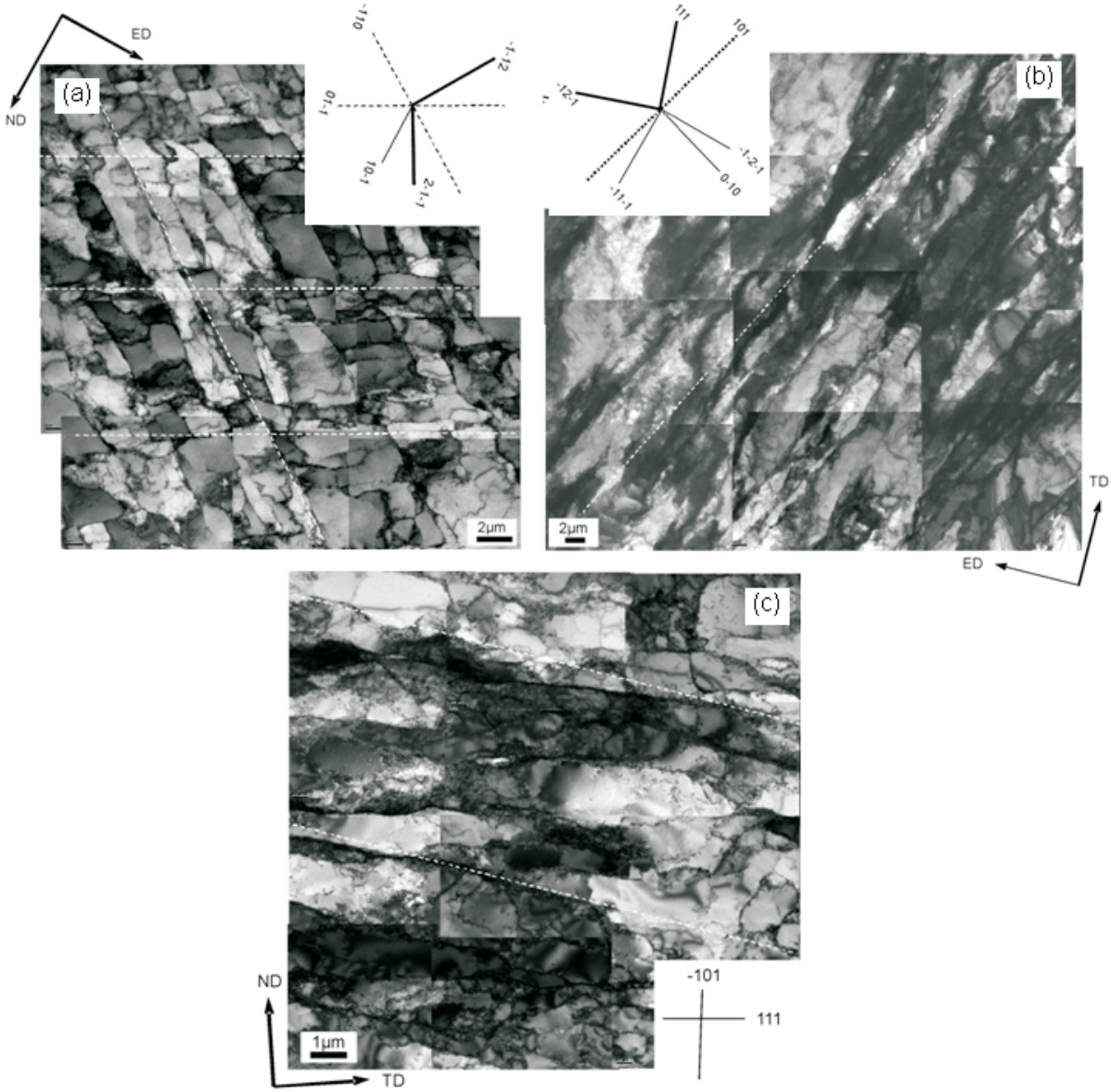

Fig. 10. Typical TEM microstructures observed after deformation of 0.55 in the sample with initial orientation within 1o deviation from the ideal position: (a) ND-ED, (b) ED-TD, and (c) ND-TD sections. TEM bright field image

3.5. Crystal of ideal brass orientation

The calculations of crystal plasticity performed using either the Taylor conditions full of constraints or the conditions for the ideal plane strain, lead to the conclusion that the ideal brass orientation is predicted to be stable. Godfrey et al. [1] show that deformation of orientations deviating 3° about certain axes, can lead, after a strain of 1.5, to the rotations of orientations up to 12° away from the ideal one. This is in accordance with our local orientation measurements by SEM and TEM, in which also misorientation axes close to the <110> crystallographic direction were found. This suggests that the majority of slips occur on the most highly stressed slip systems, since an imbalance of slip on these two systems leads to the rotation about the <110> axis. This kind of microstructure is typical for the crystallite of ideal brass orientation (within 1° deviation off the

ideal {110}<112> orientation), in which the stronger stability of the initial orientation is observed [13,14]. TEM microstructures in 3 perpendicular planes shows that microstructure composed of two sets of dislocation walls is significantly more often observed than in non-ideally-oriented crystallites. The deviation from the ideal position leads to stronger scattering of poles observed on {111} pole figures and to dominance of one of the two most active slip systems. This process is very well-described in the distribution of misorientation axes clearly showing their location close to the <112> axis.

4. Conclusions

The crystallography of extended planar dislocation boundaries in Al-0.3wt.%Mn alloy single crystal of non-ideal brass{110}<112> orientation, during channel-die compression to strains of 0.15 and 0.56 have been analyzed on all 3 sections, perpendicular to the external axes. Quantitative TEM and SEM-FEG/EBSD analyses have been applied to describe the relations between the prominent dislocation boundaries and the slip planes.

- In these ideal and non-ideal crystal orientations the applied deformation mode activates double slip of which one system predominates and leads to further rotation away from Bs. A general rotation combined with a wide orientation spread is observed after a deformation of 0.56.
- Line scan shows misorientations which frequently attain ~ 10° (in some cases even 15-20°) when the subgrains boundaries are crossed. The misorientation axes were close to TD <111> and could be correlated with <112> directions.
- The microband boundary alignment observed in this situation of 1 major and 1 minor corresponds very well to the traces of crystallographic {111} planes, on which most of the slip occurs. This is in accordance with the statement of Winther et al. [4] that boundary planes lie close to slip planes when the slip is concentrated on one or two slip planes.

Acknowledgements

H.P. gratefully acknowledges the financial support of the Ecole des Mines de Saint Etienne to the research reported in the paper.

Received: 20 December 2008.

REFERENCES

[1] A. Godfrey, D. Juul Jensen, N. Hansen, Slip pattern, microstructure and local crystallography in an aluminium single crystal of brass orientation {110}<112>, Acta mater **46**, 823-833 (1998).

[2] G. Winther, X. Huang, N. Hansen, Crystallographic and macroscopic orientation of planar dislocation boundaries-correlation with grain orientation, Acta mater. **48**, 2187-2198 (2000).

[3] G. Winther, Slip patterns and preferred dislocation boundary plane, Acta Materialia **51**, 417-429 (2003).

[4] G. Winther, X. Huang, A. Godfrey, N. Hansen, Critical comparison of dislocation boundary alignment studied by TEM and EBSD: technical issues and theoretical consequences, Acta Materialia **52**, 4437-4446 (2004).

[5] G. Winther, Scripta Materialia, Effect of grain orientation dependent microstructures on flow stress anisotropy modeling **52**, 995-1000 (2005).

[6] Z. J. Li, G. Winther, N. Hansen, Anisotropy in rolled metals induced by dislocation structure, Acta Materialia **54**, 401-410 (2006).

[7] P. J. Hurley, F. J.Humphreys, The application of EBSD to the study of substructural development in a cold rolled single-phase aluminium alloy, Acta Materialia **51**, 1087-1102 (2003).

[8] P. J. Hurley, P. S. Bate, F. J. Humphreys, An objective study of substructural boundary alignment in aluminium, Acta Materialia **51**, 4737-4750 (2003).

[9] P. S. Bate, R. D. Knutsen, I. Brough, F. J. Humphreys, The characterization of low-angle boundaries by EBSD, Journal of Microscopy **220**, 36-46 (2005).

[10] F. J. Humphreys, P. S. Bate, Measuring the alignment of low-angle boundaries formed during deformation, Acta Materialia **54**, 817-829 (2006).

[11] H. Paul, J. H. Driver, W. Wajda, Strain hardening and Microstructure Evolution in Aluminium Bicrystals Deformed in Channel-die, Materials Science and Engineering A, **A 477**, 282-294 (2008).

[12] M. Wróbel, S. Dymek, M. Blicharski, S. Gorczyca, Dislocation microstructure and texture development in rolled copper single crystals, Z. Metallkunde **85**, 415-425 (1994).

[13] Z. Jasieński, A. Piątkowski, Microstructure and texture evolution of copper single crystals in channel-die testing: the role of shear bands, Proceedings of the 9th ICSMA, Haifa, ed. D.G. Brandon et al., Freund publishing Company **2**, 1025-1030 (1991).

[14] Z. Jasieński, A. Piątkowski, Nature de bandes de cisaillement macroscopiques dans les monocristaux de cuivre sollicités en compression plane, Archives of Metallurgy, 279-292 (1993).